Effect of Materials Parameters on the Shape of Face-On Lamellae in Semi-Conducting Polymers: Insights From Qualitative Theory

Kostas Ch. Daoulas* and Anastasia A. Markina

Polymer semiconductors frequently form crystals or mesophases with lamellae, that comprise alternating layers of stacked backbones and side chains. Controlling lamellar orientation in films is essential for obtaining efficient charge carrier transport. Herein, lamellar orientation is investigated in an application-relevant setup: lamellae assembled on a substrate that strongly favors face-on orientation, but exposed to a film surface that promotes orientation along an "easy" direction, other than face on. It is assumed that the face-on order propagates from the substrate, but the lamellae bend to reduce their surface energy. A qualitative free-energy model is developed. The deformation is investigated as a function of film thickness, effective Young modulus, anchoring coefficient, and easy direction at the free surface. The calculations highlight the importance of elastic constants – lamellae can substantially deform already when Young moduli are only an order of magnitude smaller than the values that are reported for crystals. Softer Young moduli are expected when lamellar assembly occurs in a non-solidified mesophase that can be an equilibrium or (more speculatively) a transient state prior to crystallization. The alternative scenario of a two-layered film is also evaluated, where edge-on and face-on grains form, respectively, at the free surface and substrate.

1. Introduction

Soluble semiconducting polymers present significant interest[1–5] as materials for fabricating film-like active layers of electronic devices using cost-effective and scalable techniques based on solution processing. These polymers typically comprise an electrically-active conjugated backbone with flexible, electrically-inert, side chains that provide solubility. As a consequence, their (semi)crystalline phases, and many mesophases,[6] exhibit[7–9]

K. C. Daoulas, A. A. Markina
Max Planck Institute for Polymer Research
Ackermannweg 10, 55128 Mainz, Germany
E-mail: daoulas@mpip-mainz.mpg.de

The ORCID identification number(s) for the author(s) of this article can be found under https://doi.org/10.1002/marc.202300437

special lamellar order: layers of cofacially stacked backbones alternating with layers of side chains. Near an interface, such as a polymer-substrate boundary or a free film surface, there are two basic modes[10] of lamellar orientation: edge-on and face-on. As illustrated in **Figure 1**, in the former, the stacking direction is parallel to the interface, whereas in the latter it is orthogonal. Because intermolecular charge transport is most efficient along the stacking direction, edge-on lamellae are beneficial for devices requiring charge transport in the plane of the active layer, such as field-effect transistors.[1,11,12] In contrast, face-on orientation supports vertical charge transport and can be advantageous for devices where the active layer is sandwiched between two electrodes, such as organic photovoltaic cells.[1,13–15]
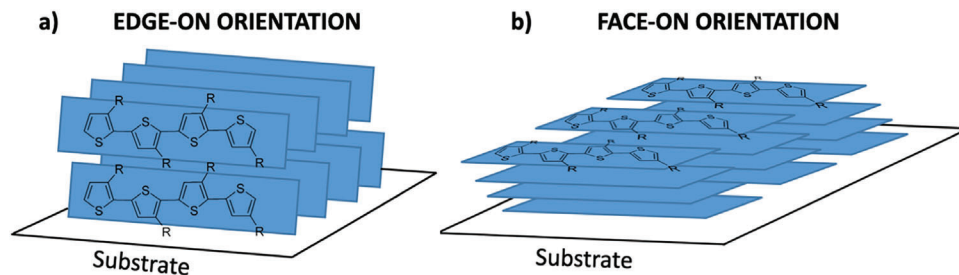
Generally, the orientation of lamellae is influenced by various factors such as details of molecular architecture,[10,11,16–18] polymer-substrate interactions[19–23] and choice of processing protocols. Typical examples are adjustment of solvent evaporation rate,[11,16] annealing,[24] control of aggregation by combining solvents,[25] application of strain,[26,27] and mechanical rubbing.[10,28,29] However, there seems to be a consensus that weakly interacting substrates,[20,21,30] such as silicon wafers,[10–12,16] thermodynamically favor edge-on lamellae whereas substrates with strong $\pi - \pi$ interactions[21,31] – graphene[18,21–23,31,32] is an important example – promote face-on orientation. Furthermore, it is believed that edge-on order is thermodynamically favored at free surfaces of films of conjugated polymers such as poly(3-hexylthiophene) (P3HT).[33] For P3HT, this experimental observation is consistent with all-atom simulations of free-standing molten films.[34]

Currently, there is only limited understanding of how competing boundary conditions – a substrate favoring face-on order and a free-surface favoring edge-on order – affect lamellae. Most of the studies, relevant for this question, concern P3HT films deposited on graphene. They report[21,22,31,35] mixed face-on and edge-on crystallites, even for thin films.[21] So far, the microstructure of these films has been interpreted only from the perspective of kinetics of crystallization. Early studies hypothesized[22] that graphene seeds face-on lamellae (heterogeneous nucleation). Recently[18] it was argued that mixed orientations are actually caused by competition between prefreezing

**ADVANCED
SCIENCE NEWS**

www.advancedsciencenews.com

**[M]acro-molecular
Rapid Communications**

www.mrc-journal.de

Figure 1. Cartoon illustrating the a) edge-on and b) face-on modes of lamellar orientation with respect to a substrate. The board-like shape marks the average plane of orientation of the conjugated polymer.

at the graphene[18] and surface freezing at the free surface.[18,33] Intriguingly, these experiments found that bromination of side chains leads[18] to sole face-on orientation in thin films. This behavior was attributed[18] to suppression of surface freezing by the chemical modification.

Whereas the kinetics of crystallization is certainly crucial, there might be additional mechanisms causing mixed lamellar orientation. For example, let us consider a case where face-on order propagates from the substrate through the entire thickness of the film. Still, near the free surface, polymers are subjected to local enthalpic and entropic effects that favor edge-on orientation. Assuming that there is sufficient molecular mobility, during structure formation, it is plausible that the face-on lamellae will bend to reduce the thermodynamic cost of an unfavorable orientation at the top of the film. Strong deformations will lead to appreciable changes of lamellar orientation through the film.

Although we are not aware of any experiments directly reporting this scenario, we speculate that it could be implicitly present in situations where gradual build-up of lamellar order occurs. One candidate are partially-ordered polymer semiconductors, known to preserve dynamical disorder.[6] Here, particularly relevant are liquid-crystalline (LC) sanidic mesophases,[9,36–38] reported to have liquid-like rheology.[39] Experiments suggest that these mesophases are relevant for conjugated polymers such as poly(2,5-bis(3-quaterdecylthiophene-2-yl)-thieno[3,2-b]thiophene) (pBTTT).[39] In some experiments, phenomenologies corresponding to sanidic LC mesophases have been reported even for short P3HT chains at elevated temperatures.[40] Another case, where this scenario could appear are thermal protocols involving prefreezing.[18] Finally, one should also take into account that even for "classical" polymer crystallization, there are theories[41] arguing that the attachment of polymer chains to growing crystals proceeds via a transient, mobile, mesomorphic layer.

Here, we assume systems where the scenario of gradual lamellar deformation holds and develop a simple analytical model to qualitatively describe this deformation. Our approach constitutes a rudimentary free-energy description of elasticity of a lamellar phase of a conjugated polymer confined between a bottom substrate that strongly favors face-on orientation and an interface at the top that promotes orientations other than face-on. Interestingly, our model, in its final form, bears an analogy to free-energy descriptions of deformed nematics sandwiched between walls that tend to orient mesogenes along different directions; hybrid aligned nematic films (HAN).[42–46] We investigate the strength of lamella deformation as a function of properties such as effec-

tive Young modulus, preferred direction and anchoring strength at the upper surface, and film thickness. Our estimations predict that in certain regions of parameter space, the deformation of lamellae can be significant.

2. Simple Free-Energy Model

To develop the free energy model, we approximate each lamella by a continuum elastic "beam", as illustrated in **Figure 2**. The length of the beam, when undeformed, equals the thickness of the film H. We require that the position of the end of the beam at $z = 0$ is fixed, whereas the opposite end at $z = H$ can be horizontally displaced parallel to the direction of lamella periodicity; in our case, this is the x-direction (see Figure 2). The thickness of the beam equals the lamella spacing d_{lam}. We assign to the beam a single Young modulus E, neglecting that lamellae are anisotropic objects and their elastic constants actually are tensors. Essentially, E is an effective Young modulus introduced for order-of-magnitude estimates only.
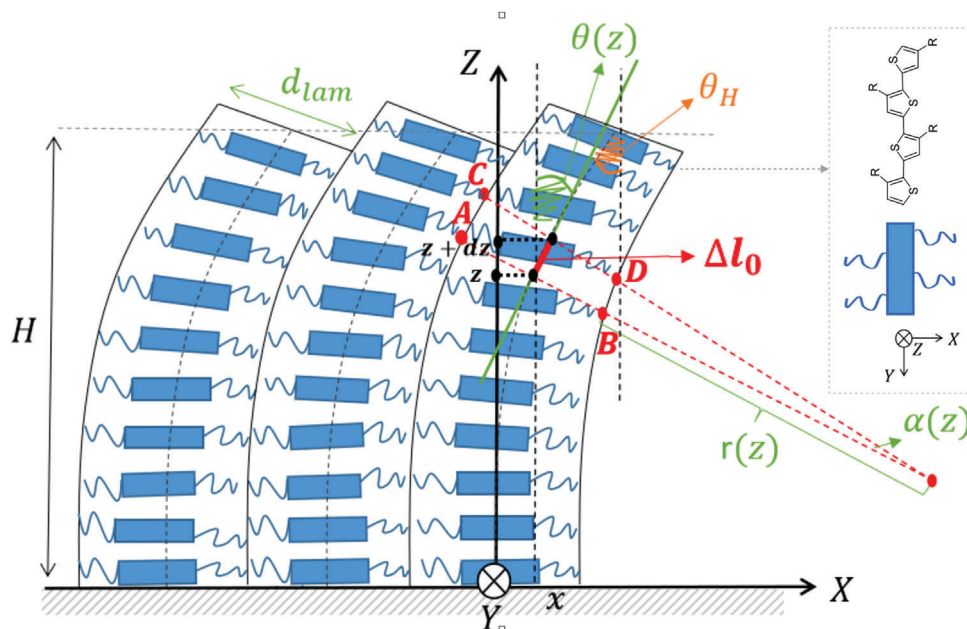
We obtain the free energy of the film per unit area $\mathcal{F}$ as a sum of two terms:

$$\mathcal{F} = \mathcal{F}_{\text{e}} + \mathcal{F}_{\text{s}} \tag{1}$$

The first term $\mathcal{F}_{\text{e}}$ accounts for the free-energy cost of deformation (per unit area) and vanishes when lamellae maintain uniform face-on order through the film. The second term $\mathcal{F}_{\text{s}}$ is the surface free energy (per unit area) that vanishes when the lamellae orient at the top surface of the film along the direction favored by this surface (this direction differs from face on). Because of strong interactions favoring face-on order at the substrate, we assume that the orientation of the lamellae at the very bottom of the film is strictly face on always. Therefore, there is no surface free-energy associated with variations of order at the substrate. The equilibrium shape of the lamellae (minimum of $\mathcal{F}$) results from a balance between $\mathcal{F}_{\text{e}}$ and $\mathcal{F}_{\text{s}}$.

Assuming that the midline of the deformed beam is also its neutral axis, the deformation can be described via the function $x(z)$ that defines the shape of the midline. However, to account for the "twisting" boundary condition at the top of the film, it is more convenient to construct the free energy as a functional of $\theta(z)$. This quantity is defined as the angle between the tangent to the midline of the beam at distance z and the film normal (i.e. the Z axis, see Figure 2).

To derive $\mathcal{F}_{\text{e}}$, we use an approach inspired by standard theories[47] of deformed beams in the limit of small

ADVANCED
SCIENCE NEWS
www.advancedsciencenews.com

[M] acro-
molecular
Rapid Communications
www.mrc-journal.de

Figure 2. Cartoon explaining the main scenario of lamella deformation investigated in our study. The semiconducting polymers are oriented with their long molecular axis orthogonal to the page, so that the blue rectangles are side views of their conjugated backbones with aromatic rings. The layers of the $\pi - \pi$ stacked backbones are separated by layers of side chains, indicated by blue thin lines. There is some irregularity in the position and orientation of rectangles, and side chains are drawn wiggling, to indicate partial order as well as molecular mobility, i.e. the structure is not solidified. The inset on the right clarifies the graphical representation of the conjugated polymers and explains their orientation with respect to the laboratory coordinate frame. The lamellae are assembled on a substrate strongly favoring face-on orientation, which propagates into the film. However, the free surface of the film promotes orientation along an "easy" direction, other than face on. Hence, the face-on lamellae can bend to reduce their surface energy at the free surface at some expense of elastic energy. The orientation of lamellae at distance z from the substrate is quantified via the angle $\theta(z)$ between the tangent to their midline and the film normal (the Z axis). Accordingly, θ_H is the equilibrium orientation of lamellae at the free surface. Because the equilibrium shape of lamellae stems from a balance between elastic and surface energy, θ_H, in general, deviates from the easy direction $\bar{\theta}_H$ (not shown here, see main text for details). The period of lamellae and film thickness are, respectively, d_{lam} and H. The remaining elements of the figure are used when constructing the elastic part of the free energy and are defined in the main text.

deformations; this corresponds to $x'^2 \ll 1$, where $x' \equiv dx/dz$. Then, the radius of curvature of the midline at z is[48] $r(z) = (1 + x'^2)^{3/2}/x'' \simeq 1/x''$ (see Figure 2). Here $x'' \equiv d^2x/dz^2$. Let AB and CD be the cross-sections of the beam that are orthogonal to the midline at points with coordinates z and $z + dz$. The length of the midline between these two points is Δl_0. The extrapolations of AB and CD intersect at angle $\alpha(z)$. Defining a local axis Ξ oriented along AB, the local strain at distance ξ from the midline is $\epsilon = [(r(z) + \xi)\alpha(z) - r(z)\alpha(z)]/r(z)\alpha(z) \simeq \xi x''$. Neglecting changes of volume during deformation, the strain energy stored in a slice with volume $dV = d\xi \Delta l_0 L_y$ is $dU = (E/2)\epsilon^2 dV$; here, L_y is the width of the beam (the dimension orthogonal to the drawing plane of Figure 2). Considering that $\Delta l_0 = dz\sqrt{1 + x'^2} \simeq dz$, the total elastic energy equals:

$$U = \frac{EL_y}{2} \int_{-\frac{d_{lam}}{2}}^{\frac{d_{lam}}{2}} d\xi \int_0^H (x''\xi)^2 dz = \frac{EL_y}{2} \frac{d_{lam}^3}{12} \int_0^H x''^2 dz \quad (2)$$

Taking into account that $x' = \tan\theta(z) \simeq \theta(z)$ and $L_y d_{lam}$ is the area of the beam cross-section, Equation (2) straightforwardly leads to:

$$\mathcal{F}_e = \frac{K}{2} \int_0^H \left(\frac{d\theta(z)}{dz}\right)^2 dz, \quad \text{where} \quad K = \frac{E}{12} d_{lam}^2 \quad (3)$$

We define $\mathcal{F}_s$ by:

$$\mathcal{F}_s = \frac{W}{2} \sin^2\left(\theta(H) - \bar{\theta}_H\right) \quad (4)$$

This choice is inspired by free energies used to describe surface anchoring of mesogenes in nematic films.[42] The angle $\bar{\theta}_H$ indicates the direction of anchoring preferred at the upper surface, named also[49] "easy direction". For example, for surfaces favoring perfect edge-on orientation $\bar{\theta}_H = \pi/2$. The thermodynamic cost of deviations of the lamella orientation at the top of the film from the easy direction, i.e. the deviation of $\theta(H)$ from $\bar{\theta}_H$, is controlled by the anchoring coefficient W.

The mathematical structure of $\mathcal{F}$, obtained after substitution of $\mathcal{F}_e$ and $\mathcal{F}_s$ into Equation (1), is identical to simple free-energy models[42,50] of hybrid nematic films. However, the ingredients of the free energies have different physical meaning. In the nematic free energy, $\theta(z)$ is the angle between the nematic director and the film normal. Furthermore, the elasticity term is the Frank–Oseen elastic energy under the assumption that all Frank constants equal K. Keeping in mind these conceptual differences, we can, nevertheless, benefit from the mathematical equivalence of the models and directly use some of the results that have been obtained[42,50] for nematics.

ADVANCED
SCIENCE NEWS
www.advancedsciencenews.com

[M] acro-
molecular
Rapid Communications
www.mrc-journal.de

The profile $\theta(z)$ that minimizes $\mathcal{F}$ is a linear function[42,50]:

$$\theta(z) = \theta_H \frac{z}{H} \tag{5}$$

The constant θ_H specifies the equilibrium value of $\theta(H)$ and fulfils[42,50] the boundary condition:

$$\theta_H + \frac{H}{2\bar{L}} \sin\left(2(\theta_H - \bar{\theta}_H)\right) = 0, \quad \text{where} \quad \bar{L} = \frac{K}{W} \tag{6}$$

The characteristic length $\bar{L}$ is analogous to the anchoring extrapolation length in nematics.[49] In the following, we determine θ_H by solving the transcendental Equation (6) numerically, using a standard bracketing scheme.[51]

One can obtain the shape of the midline by substituting $\theta(z)$ in Equation (5) by x' and integrating with the boundary condition $x(0) = 0$. It turns out to be a simple parabolic function:

$$x(z) = \frac{\theta_H}{2H} z^2 \tag{7}$$

Since our theoretical description is only valid for small deformations, it is important to perform a consistency check. Based on Equation (7), we find that the maximum value of x'^2 is θ_H^2. Hence, the relative error of the approximation $\sqrt{1 + x'^2} \simeq 1$ is on the order of $\theta_H^2/2$. For $\theta_H = \pi/9$ (equivalently 20°) this estimate corresponds to about 6% of error. Therefore, as a rule of the thumb, we can assume that our theory is applicable to deformations where $\theta(z) \leqslant \pi/9$.

For the following discussion, we will also need the free energy of the film. After substituting Equation (5) into $\mathcal{F}_e$ and $\mathcal{F}_s$, it is straightforward to show that:

$$\mathcal{F} = \frac{K}{2} \frac{\theta_H^2}{H} + \frac{W}{2} \sin^2\left(\theta_H - \bar{\theta}_H\right) \tag{8}$$

Here θ_H fulfils Equation (6). For solutions with $\theta_H > 0$ $\mathcal{F}$ describes the free energy of the deformed state, $\mathcal{F}_{df}$, whereas for $\theta_H = 0$ it reduces to the free energy of the undeformed state, $\mathcal{F}_{ud} = \frac{W}{2} \sin^2(\bar{\theta}_H)$.

3. Results and Discussion

3.1. Deformation: Generic Properties

Because $\theta(z)$ increases monotonously with z, Equation (5), the maximum deformation occurs at $z = H$ and is quantified by θ_H calculated via Equation (6). Equation (6) demonstrates that the deformation is determined by two generic parameters: the easy angle $\bar{\theta}_H$ and the ratio of film thickness to the extrapolation length, $H/\bar{L}$. This point has been extensively discussed in the framework of a mathematically equivalent description of nematic films.[42,52] For the special case $\bar{\theta}_H = \pi/2$ the lamellae remain undeformed when $H \leq \bar{L}$, i.e. Equation (6) has only one trivial solution, $\theta_H = 0$ (cf. with analysis in nematic films[42,52]). The absence of a second solution $\theta_H > 0$ follows straightforwardly by demonstrating that the LHS of Equation (6) has a positive derivative. For $\bar{\theta}_H = \pi/2$ the deformed state appears, Equation (6) has a second, non-trivial, solution, only when $H > \bar{L}$. The deformed state has

a lower free energy than the undeformed state and is favored thermodynamically. This conclusion follows[42] by demonstrating that for $H > \bar{L}$ the solution $\bar{\theta}_H = 0$ is unstable. It corresponds to a maximum of $\mathcal{F}$, where $\frac{d^2\mathcal{F}}{d\theta_H^2}|_{\theta_H=0} > 0$.

When $\bar{\theta}_H < \pi/2$, the deformed state exists (and is favored thermodynamically) even for $H \leq \bar{L}$. We illustrate this point in **Figure 3**a, by presenting θ_H obtained from the numerical solution of Equation (6) as a function of the generic parameter $H/\bar{L}$ for a few representative values $\bar{\theta}_H = 20°, 45°, 60°$, and $89°$ (for convenience, hereafter all angles are given in degrees). For reference, in Figure 3a we also present the plot of the deformation for $\bar{\theta}_H = 90°$ (red dashed line). Interestingly, we observe that in the region $H/\bar{L} < 1$ the magnitude of deformation depends on $\bar{\theta}_H$ non-monotonously. That is, at given $H/\bar{L}$ the deformation first increases as a function of $\bar{\theta}_H$ and then decreases again to vanish at $\bar{\theta}_H = 90°$. This behavior is illustrated in Figure 3b, where we present the deformation θ_H as a function of the easy angle $\bar{\theta}_H$ for three representative choices of $H/\bar{L}$ (all smaller than unity). The non-monotonic behavior is evident in all plots. The value of the easy angle at which the deformation is maximized (the peak of the plots) shifts toward $\bar{\theta}_H = 90°$ as $H/\bar{L}$ approaches unity.

In summary, from the generic plots in Figure 3 we can already conclude that in films, where $H < \bar{L}$, the deformation of lamellae is maximized for free surfaces that favor easy angles with intermediate values and not perfect edge-on orientation ($\bar{\theta}_H = 90°$).
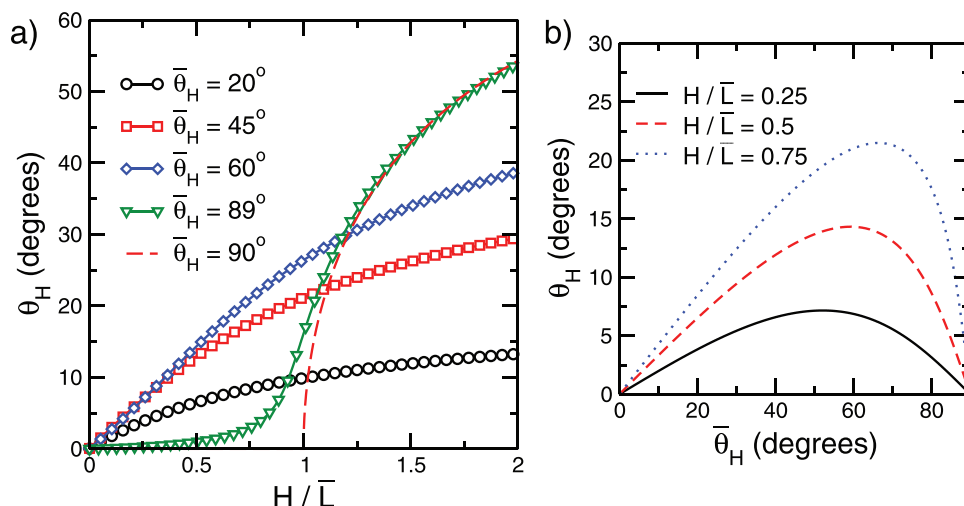
3.2. Deformation: Solid-State Scenario for Young Modulus

To connect to actual materials, we must recast the predictions of the simple theory in a way that explicitly resolves the effect of the different material-specific parameters. To this end, we consider two film thicknesses $H = 10$ and 50 nm, which are representative of the thicknesses encountered in actual active layers. To specify $\bar{L}$ we need to estimate K and W (see definition in Equation (6)). The estimation of K (see Equation (3)) requires as an input realistic values for lamella spacing and effective Young modulus. In many conjugated polymers the lamella spacing lies between 1.5 and 3 nm; for example, this is a typical range of values that has been reported in poly(alkyl thiophenes) with different lengths of side chains.[8,53] For our calculations, without loss of generality, we set $d_{lam} = 1.5$ nm. For example, considering $d_{lam} = 3$ nm would only increase K by a factor of four without qualitatively affecting our calculations (cf. Equation (3)). The choice of the order of magnitude of E plays a central role in our study and is discussed in the following paragraphs.

Because typical anchoring strengths for conjugated polymers at the free surface are unknown, we treat W as a free parameter. We assume that $10^{-6} \leqslant W \leqslant 10^{-3}$ J m^{-2}, which is a typical range for nematic LC.[50] It is instructive to compare this range of values with the thermal energy, $k_B T$ (where k_B is the Boltzmann constant and T the temperature). For example, for $T = 500$ K, $W = 10^{-3}$ J m^{-2} is about $0.14\,k_B T$ nm^{-2}, demonstrating that the surface energy $\mathcal{F}_s$ is small.

An indirect indication that our assumptions for the orders of magnitude of W at the free surface are plausible, stems from a back-of-the-envelope estimation of the energy difference $\Delta\mathcal{E}$ between face-on and edge-on orientations of P3HT on graphene. Because the preference for face-on orientation on graphene is

ADVANCED
SCIENCE NEWS
www.advancedsciencenews.com

[M]acro-
molecular
Rapid Communications
www.mrc-journal.de

Figure 3. a) Deformation of lamellae at the top of the film, quantified by the angle θ_H (cf. Figure 2), presented as a function of the generic parameter $H/\bar{L}$, where H is the film thickness and $\bar{L}$ the extrapolation length (for definition see main text). Several representative easy angles $\bar{\theta}_H$ at the free surface are considered, as indicated by the labels. The plot for $\bar{\theta}_H = 90°$ is singled out by a red dashed line, because in this special case lamellae remain undeformed when $H/\bar{L} \leq 1$. b) Dependence of deformation of lamellae at the top of the film, θ_H, on the easy angle $\bar{\theta}_H$ for selected cases of $H/\bar{L}$, all smaller than unity.

strong,[18,21–23,31,32] one anticipates that $\Delta\mathcal{E}$ provides an upper boundary estimate, i.e. W should be clearly smaller than $\Delta\mathcal{E}$. In quantum chemistry calculations[32] the difference of binding energies between a face-on and edge-on orientation, per P3HT monomer, was found to be $\Delta E = 1.19$ eV. A rough estimate of the corresponding difference in energy per unit area is given by $\Delta\mathcal{E} = \rho\Delta E\Delta h$, where ρ is the number density of monomers and Δh the characteristic thickness of the interfacial monomer layer. Substituting $\rho \sim 4$ monomers nm^{-3} (this is, approximately, the monomer number density[7,37,54] in P3HT) and $\Delta h \sim 0.1 - 1$ nm leads to $\Delta\mathcal{E} = 0.076 - 0.76$ J m^{-2}.

At a first glance, it is reasonable to consider a Young modulus on the order of $E = 1$ GPa. This magnitude has been reported, for example, in experimental studies of P3HT in solid state, i.e. semicrystalline samples[55] or nanofibers[56] around room temperature. Experiments that have explicitly resolved[56] the anisotropy of Young modulus along the direction of π-conjugated backbone (the Y axis in Figure 2) and lamellar periodicity (the X axis in Figure 2) found this magnitude for the largest component that corresponded to the lamellar periodicity.

In the semi-log graph of **Figure 4**a we present $\bar{L}$ (black circles) as a function of W for $E = 1$ GPa. For all W, $\bar{L}$ significantly exceeds the largest film thickness $H = 50$ nm considered in our study (red dashed line in Figure 4a), e.g. for the largest anchoring coefficient, $W = 10^{-3}$ J m^{-2} we have $\bar{L} \simeq 187$ nm, which approximately corresponds to $H/\bar{L} \simeq 0.25$ in the generic plots of Figure 3. Therefore, when the easy angle is $\bar{\theta}_H = 90°$, we conclude that, for $E = 1$ GPa, face-on order of lamellae will propagate through the film without any deformation even for $H = 50$ nm, let alone $H = 10$ nm.
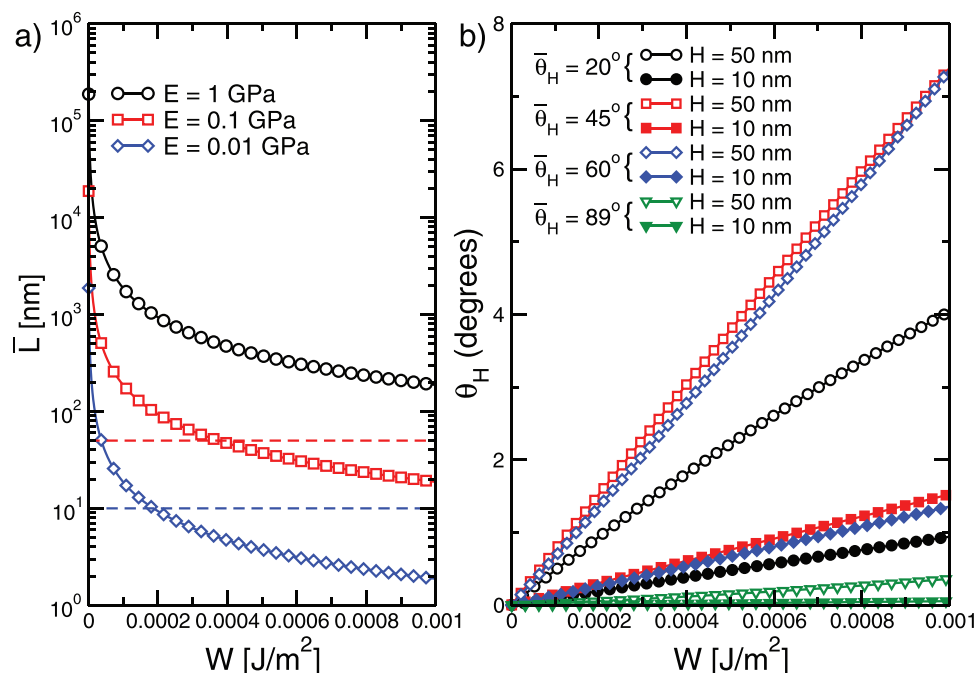
As has been discussed in Section 3.1, in the most general case $\bar{\theta}_H < 90°$ deformation takes place even when $H < \bar{L}$. In Figure 4b, we consider the same values of $\bar{\theta}_H$ as in the generic plots of Figure 3a. For these easy angles, we present θ_H calculated numerically for $E = 1$ GPa as a function of W, for films with $H =$ 10 nm (solid symbols) and 50 nm (open symbols). Even for the case of the strongest anchoring, $W = 10^{-3}$ J m^{-2} the maximum deformations for $H = 10$ and $H = 50$ nm are, respectively, about $\theta_H \simeq 2°$ and $8°$ only.

Based on Figure 4b, we conclude that for the scenario of "solid-state-like" elasticity, where the extrapolation length substantially exceeds the typical film thicknesses, the deformations of lamellae in response to competing boundary conditions are very small and can be neglected in practice. Interestingly, quantum chemistry calculations for oligomers of P3HT[57] and poly(3,4-ethylenedioxythiophene) (PEDOT)[58] suggest that the Young modulus along the direction of the backbone is actually the highest, in contrast to the aforementioned experiment,[56] with an order of magnitude $\sim 10 - 100$ GPa. This difference does not affect our qualitative conclusions regarding the smallness of deformations for "solid-state-like" elasticity.

3.3. Deformation: Mesophase Scenario for Young Modulus

However, in this work we are considering a pathway that assumes sufficient molecular mobility during the build-up of lamellae. We believe that within this assumption, $E = 1$ GPa overestimates the Young modulus. Because the molecular mobility is not quenched during ordering, the film should be seen rather as a highly ordered mesophase. Representative molecular-level illustrations of the structure of such highly ordered mesophases in conjugated polymers are available[37,59–61] from mesoscopic simulations. Highly ordered liquid crystals, such as smectics, have smaller elastic constants than crystals and behave as[62,63] "weak solids". For example, in some smectics the layer-compression modulus (the Young modulus along the periodic direction) was found[64] to be on the order of 0.01 GPa. Therefore, in this section we estimate the deformation of lamellae for $E = 0.1$ GPa

ADVANCED
SCIENCE NEWS

www.advancedsciencenews.com

[M] acro-
olecular
Rapid Communications

www.mrc-journal.de

Figure 4. a) Extrapolation length $\bar{L}$ as a function of the anchoring strength W for the three effective Young moduli considered in our study. The horizontal blue and red dashed lines, mark, respectively, the two representative film thicknesses $H = 10$ and 50 nm. b) Deformation of lamellae at the top of the film, quantified by the angle θ_H calculated as a function of W, assuming a solid-state-like Young modulus $E = 1$ GPa. Several representative easy angles $\bar{\theta}_H$ at the free surface are considered, as indicated by the labels. Here, we do not plot θ_H for the case $\bar{\theta}_H = 90°$ (cf. Figure 3) because, for all W, the film thicknesses H addressed in our work are smaller than the extrapolation length $\bar{L}$. Therefore the lamellae do not deform.

(a Young modulus that is only one order of magnitude smaller than in the solid-like case) and $E = 0.01$ GPa.

First, in Figure 4a we demonstrate $\bar{L}$ calculated as a function of W for these two values of E (red squares and blue rhombi respectively). We observe that for $E = 0.1$ GPa there is a region of W for which $\bar{L}$ is smaller than our largest film thickness $H = 50$ nm (dashed red line). Based on Section 3.1, strong deformations are expected in this case. Furthermore, for $E = 0.01$ GPa there is a region of W where $\bar{L}$ drops below even $H = 10$ nm (dashed blue line).

Next, in **Figure 5**a,b we present $\bar{\theta}_H$ calculated for $E = 0.1$ GPa and 0.01 GPa, respectively. Each of the two figures presents plots for $H = 10$ nm (solid symbols) and $H = 50$ nm (open symbols), and for the same values of $\bar{\theta}_H$ as in Figures 3a, 4b. For reference, in Figure 5a we also present the deformation for $H = 50$ nm and $\theta_H = 90°$ (dashed red line), where we see a clear transition from the undeformed to the deformed state. For the "softer" mesophase $E = 0.01$ GPa this transition occurs even in thin $H = 10$ nm films (blue dashed line). Overall, we observe that reducing E just by one or two orders of magnitude, comparing to the Young modulus expected in a solid state, increases substantially the deformation of lamellae. Especially, in the softer mesophase θ_H starts to converge to the easy direction $\bar{\theta}_H$ as W approaches its largest values.
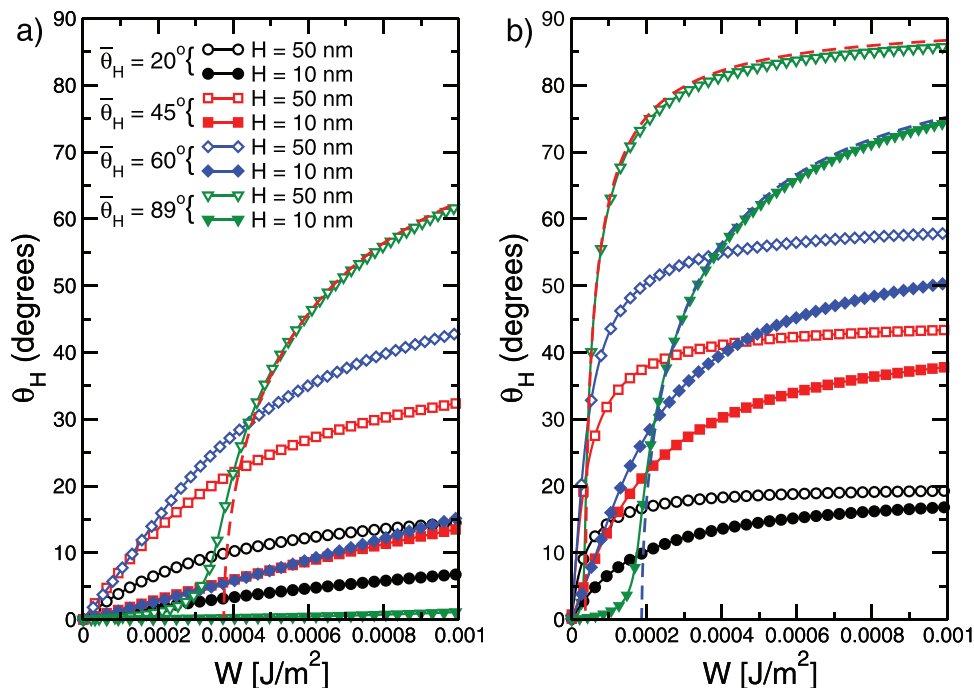
Certainly, in a large part of parameter space the deformations shown in Figure 5 exceed 20° – the qualitative threshold value for which our theory is formally valid (cf. Section 2). Large deformations may be relaxed by morphological changes not captured by the simple free-energy model, such as defects in lamella order.

Still such rearrangements will destroy perfect face-on lamellae. Hence, we do not expect that the limitations of our theory affect our main conclusion that for "mesophase-like" elasticity competing boundary conditions can significantly modify lamellar order.

3.4. Two-Layered Structure

There is, however, one possible rearrangement of morphology that incorporates bending deformation and can be also investigated using the simple free-energy model. As illustrated in **Figure 6**, in this rearrangement, the face-on lamellae do not grow continuously until the free surface. They disrupt, at some distance $H_g < H$ from the substrate, to create an upper layer of lamellae with $\pi - \pi$ stacks parallel to the easy direction $\bar{\theta}_H$. Thus, the surface energy of the upper layer is fully optimized. For the sake of a qualitative discussion, here we assume that $\bar{\theta}_H = 90°$. We will indicate the upper layer as "layer A" whereas the underlying layer with the face-on lamellae will be denoted as "layer B". Of course, the layers A and B are composed of one type of molecules, but, due to the discontinuity in orientation, they are two distinct grains. There are two basic questions: i) Can the two-layered morphology be more favorable thermodynamically than a single layer of face-on lamellae, either deformed or undeformed, spanning the entire film ? and ii) Where is the grain boundary, or, what is the value of H_g ?

To address these questions, we notice that the grain boundary acts as an effective upper surface for the layer B of face-on lamellae. We approximate the surface free energy γ of the grain

ADVANCED
SCIENCE NEWS
www.advancedsciencenews.com

{M}acro-
molecular
Rapid Communications
www.mrc-journal.de

Figure 5. Same as in Figure 4b but assuming a "softer" Young modulus: a) $E = 0.1$ GPa and b) $E = 0.01$ GPa. In contrast to $E = 1$ GPa (cf. Figure 4b), for these E there is a region of anchoring strengths W for which the extrapolation length $\bar{L}$ exceeds one or both representative film thicknesses considered in our study. Therefore, the lamellae can deform even for $\bar{\theta}_H = 90°$. For $E = 0.1$ GPa, in panel a), deformation is possible for $H = 50$ nm and is shown with a red dashed line. For $E = 0.01$ GPa, in panel b), deformations are possible for $H = 10$ and $H = 50$ nm and are shown with blue and red dashed lines, respectively.

boundary by the expression used for $\mathcal{F}_s$, Equation (4), but with an easy angle $\bar{\theta}_g$ and an anchoring coefficient W_g. The most favorable thermodynamically configuration for the relative orientation of two grains is the situation where they are identically oriented, that is, they "merge" and erase the interface. For instance, such fusion of parallel grains has been observed in Molecular Dynamics (MD) all-atom simulations of a small-molecule organic semiconductor at room temperature.[65] Hence, $\bar{\theta}_g = 90°$. Accordingly, the anchoring coefficient W_g determines the thermodynamic penalty for the orientational mismatch of two grains.

We are not aware of any experiments or molecular-based simulations quantifying the surface tension between grains of lamellae in conjugated polymers, but can make an order-of-magnitude estimate. Let l be the width of the grain boundary. Then γ/l is the density of the free-energy cost stored in the interface. Because grain boundaries are spontaneously formed during crystallization – including grains with strong orientational mismatch – it is reasonable to assume that γ/l is at most on the order of the density of the thermal energy of monomers. If the number density of monomers is ρ, we obtain $\gamma \lesssim l\rho k_B T$. Requiring that $W_g \sim \gamma$, and substituting typical values $l \sim 0.1$ nm and $\rho \sim 4$ monomers nm^{-3} (the monomer number density in P3HT) we estimate $W_g \lesssim 0.4\,k_B T\,\text{nm}^{-2}$. Recalling that the largest anchoring coefficients W are also on the order of 0.1 $k_B T\,\text{nm}^{-2}$, our simple calculation demonstrates that both possibilities should be considered: $W_g > W$ and $W_g < W$.

The free energy of the two-layered film, $\mathcal{F}^{(2)}$ is estimated as follows. Because the stacks of the lamellae in layer A are oriented parallel to the free surface, one can assume, to a first approximation, that the layer A is always undeformed. Hence, $\mathcal{F}^{(2)}$ is entirely determined by the free energy of layer B:
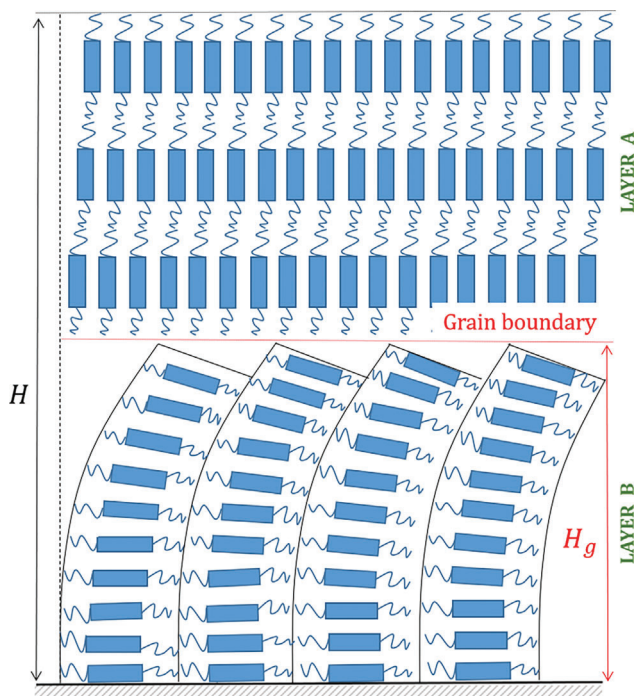
$$\mathcal{F}^{(2)} = \frac{K}{2}\frac{\theta_g^2}{H_g} + \frac{W_g}{2}\sin^2\left(\theta_g - \frac{\pi}{2}\right) \tag{9}$$

Here θ_g fulfils an equation similar to Equation (6), where the relevant parameters are $\bar{\theta}_g = \pi/2$, H_g, and $\bar{L}_g = K/W_g$; the latter is the extrapolation length of the grain boundary.

Let us first consider situations where $W_g > W$, equivalently $\bar{L}_g < \bar{L}$, and distinguish three cases. They are demonstrated in the upper row of **Figure 7**. In the first case $H < \bar{L}_g < \bar{L}$ (see Figure 7a). The layer B is undeformed for any possible H_g, so that $\mathcal{F}^{(2)}$ reduces to the free energy of the undeformed state $\mathcal{F}_{ud}^{(2)} = W_g/2$. In our main scenario, the face-on lamellae are also undeformed, so that $\mathcal{F} = \mathcal{F}_{ud} = W/2$. Since $\mathcal{F}_{ud}^{(2)} > \mathcal{F}_{ud}$ the formation of a two-layered film is not favored thermodynamically.

In the second case $\bar{L}_g < H < \bar{L}$ (see Figure 7b). Here, we have only to consider $\bar{L}_g < H_g < H$, because the free energy of a deformed layer B $\mathcal{F}_{df}^{(2)}$ will be always smaller than $\mathcal{F}_{ud}^{(2)}$ (obtained when $H_g \leq \bar{L}_g$). Furthermore:

$$\frac{d\mathcal{F}_{df}^{(2)}}{dH_g} = \frac{K}{H_g}\frac{d\theta_g}{dH}\underbrace{\left[\theta_g + \frac{W_g}{2\bar{L}_g}\sin\left(2\left(\theta_g - \frac{\pi}{2}\right)\right)\right]}_{=0} - \frac{K\theta_g^2}{2H_g^2} \tag{10}$$

ADVANCED
SCIENCE NEWS

www.advancedsciencenews.com

[M]acro-
molecular
Rapid Communications

www.mrc-journal.de

Figure 6. Illustration of a scenario, alternative to the simple bending of face-on lamellae (cf. Figure 2). The face-on lamellae do not grow continuously until the free surface but disrupt, at some distance $H_g < H$ from the substrate. An upper layer (grain) appears, where the $\pi - \pi$ stacks of the lamellae are parallel to the easy direction $\bar{\theta}_H$. In the lower layer, the face-on lamellae might still bend to optimize the surface energy at the grain boundary (located at $z = H_g$). The upper and the lower grains are indicated as "layer A" and "layer B", respectively.

Because $\mathcal{F}_{df}^{(2)}$ is a monotone decreasing function of H_g, the grain boundary must be as close as possible to H. That is, $H_g = H - d_{lam}$, or, approximately, $H_g \simeq H$. Therefore, we must compare the free energies $\mathcal{F}_{df}^{(2)} = \frac{K}{2}\frac{\theta_g^2}{H} + \frac{W_g}{2}\sin^2(\theta_g - \frac{\pi}{2})$ and $\mathcal{F}_{ud} = W/2$. We substitute $H_g = H$ into $\mathcal{F}^{(2)}$ and notice that it is a monotone increasing function of W_g:

$$\frac{d\mathcal{F}^{(2)}}{dW_g} = \frac{K}{H}\frac{d\theta_g}{dW_g}\underbrace{\left[\theta_g + \frac{W_g}{2\bar{L}_g}\sin\left(2\left(\theta_g - \frac{\pi}{2}\right)\right)\right]}_{=0} + \frac{1}{2}\sin^2\left(\theta_g - \frac{\pi}{2}\right)$$

(11)

Mathematically, $\mathcal{F}_{ud} = W/2$ is a special case (i.e., if $W = W_g$) of $\mathcal{F}^{(2)}$ considered in Equation (11). Because $W_g > W$, it follows that $\mathcal{F}_{df}^{(2)} > \mathcal{F}_{ud}$. The formation of a two-layered film is again unfavorable.

In the last case, $\bar{L}_g < \bar{L} < H$ (see Figure 7c). Now it is necessary to compare the free energy of a deformed layer B, $\mathcal{F}_{df}^{(2)} = \frac{K}{2}\frac{\theta_g^2}{H} + \frac{W_g}{2}\sin^2(\theta_g - \frac{\pi}{2})$, (recall that $H_g \simeq H$) with the free energy of deformed face-on lamellae in our main scenario, $\mathcal{F}_{df} = \frac{K}{2}\frac{\theta_H^2}{H} + \frac{W}{2}\sin^2(\theta_H - \frac{\pi}{2})$. As before, based on Equation (11), we conclude that $\mathcal{F}_{df}^{(2)} > \mathcal{F}_{df}$ and the two-layered morphology is unfavorable thermodynamically.

We now consider situations where $W_g < W$, equivalently $\bar{L}_g > \bar{L}$, and distinguish three cases. They are demonstrated in the bottom row of Figure 7. In the first case, $H < \bar{L} < \bar{L}_g$ (see Figure 7d). Since the layer B in the two-layered structure and the face-on lamellae in our main scenario are undeformed, we compare $\mathcal{F}_{ud}^{(2)} = W_g/2$ and $\mathcal{F}_{ud} = W/2$. Obviously, $\mathcal{F}_{ud}^{(2)} < \mathcal{F}_{ud}$ and the two-layered structure is now favorable. Furthermore, because $\mathcal{F}_{ud}^{(2)}$ does not depend on H_g, the grain boundary can be anywhere, i.e. the thickness of layer A is arbitrary.

Next, we consider $\bar{L} < H < \bar{L}_g$ (see Figure 7e). Because the face-on lamellae in our main scenario deform but the layer B in the two-layered structure is undeformed, we compare $\mathcal{F}_{df} = \frac{K}{2}\frac{\theta_H^2}{H} + \frac{W}{2}\sin^2(\theta_H - \frac{\pi}{2})$ with $\mathcal{F}_{ud}^{(2)} = W_g/2$. As previously, we argue that $\mathcal{F}_{ud}^{(2)}$ and $\mathcal{F}_{df}$ are, mathematically, special cases of $\mathcal{F}$. Because $\mathcal{F}$ is a monotone increasing function of W (similarly to Equation (11)) and $W_g < W$, we conclude that $\mathcal{F}_{ud}^{(2)} < \mathcal{F}_{df}$. Again, a two-layered structure is favored thermodynamically and the grain boundary can be anywhere in the film.

In the last case, $\bar{L} < \bar{L}_g < H$ (see Figure 7f). The face-on lamellae in our main scenario and layer B in the two-layered film are deformed. Since in this situation $H_g \simeq H$, we compare $\mathcal{F}_{df} = \frac{K}{2}\frac{\theta_H^2}{H} + \frac{W}{2}\sin^2(\theta_H - \frac{\pi}{2})$ with $\mathcal{F}_{df}^{(2)} = \frac{K}{2}\frac{\theta_g^2}{H} + \frac{W_g}{2}\sin^2(\theta_g - \frac{\pi}{2})$. Since $W_g < W$, we conclude that a two-layered film is favored thermodynamically also in this case. Because now the layer B deforms, the grain boundary approaches the free surface of the film as close as possible, that is, essentially the layer A is a monolayer.

In summary, when $W_g > W$ a two-layered film will not form, at least as an equilibrium structure. Intuitively, this conclusion is expected: one cannot reduce the free-energy cost by "replacing" one interface, the free film surface, by another, the grain boundary, that has a higher thermodynamic penalty for mismatch between the lamella orientation and the easy direction. In contrast, a two-layered film is favored thermodynamically when $W_g < W$. For the location of the grain boundary, the relationship between $\bar{L}_g$ and H is crucial: when $H < \bar{L}_g$ the grain boundary can be anywhere, whereas for $H > \bar{L}_g$ the grain boundary is as close as possible to the free surface.
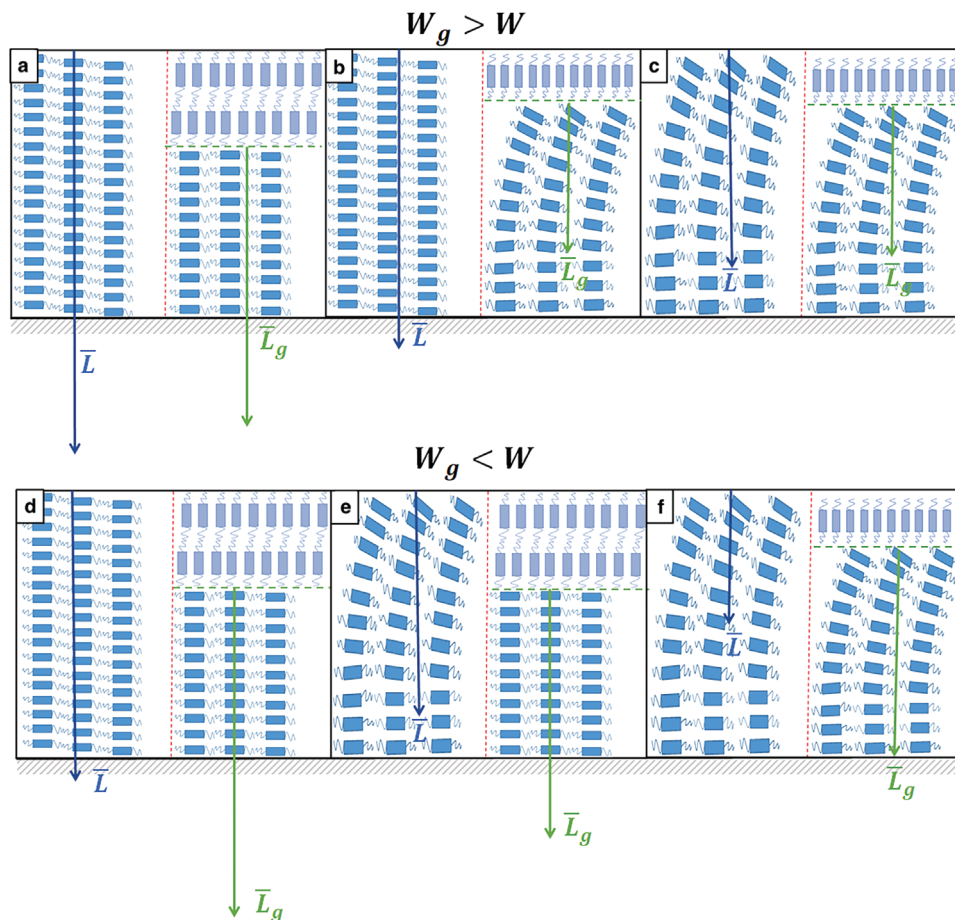
3.5. Anticipated Effects of Elastic Anisotropy

We conclude the presentation of results by commenting upon how our simplified description of elasticity might affect the theoretical predictions.

The free-energy cost of deformation $\mathcal{F}_e$, Equation (3), is constructed by drawing an intuitive analogy between the bending of lamellae and the deformation of a continuum beam. This approach is not explicitly considering the picture of the deformation of the anisotropic, generally 3D, "lattice-like" lamellar structure. Free-energy models based on such more detailed analysis will be more complex functionals of quantifiers of strain than our $\mathcal{F}$. In general, their minimization is expected to predict deformations that differ from the linear profile of Equation (5) (or its equivalent Equation (7)).

This point is well illustrated in the simpler example of HAN, where influences of elastic anisotropy have been theoretically explored[42,66] by allowing bending and splay constants to be different. Indeed, in this case, the equilibrium profile of the nematic

**ADVANCED
SCIENCE NEWS**

www.advancedsciencenews.com

{M}acro-
molecular
Rapid Communications

www.mrc-journal.de

Figure 7. The six panels illustrate the cases considered during the comparison of the free energies of a film with a single layer of face-on lamellae (left columns) and of a film with two grains (right columns). For the panels shown in the upper row $W_g > W$ and the three characteristic length scales compare as follows: a) $H < \bar{L}_g < \bar{L}$, b) $\bar{L}_g < H < \bar{L}$, and c) $\bar{L}_g < \bar{L} < H$. For the panels shown in the bottom row $W_g < W$ and the three characteristic length scales compare as follows: d) $H < \bar{L} < \bar{L}_g$, e) $\bar{L} < H < \bar{L}_g$, and f) $\bar{L} < \bar{L}_g < H$.

director field has[42,66] a more complicated dependence on height z than linear. The shift of the critical film thickness (at which the transition from the non-deformed to the deformed state occurs) to values other than $H = \bar{L}$ is another effect of elastic anisotropy found HAN. Hence, most likely, the location and details of the transition, predicted by more complex models of lamellar deformation, will change as well.

However, we expect that employing more complex theories will not affect the magnitude predicted for the deformations of lamellae, especially as a function of the order of magnitude of elastic constants – one of the central messages of our study.

4. Conclusion

We investigated the shape of lamellae of conjugated polymers in films where the solid substrate strongly favors face-on orientation, whereas the free surface promotes orientation along an "easy" direction, other than face on. Our study focused on a scenario where molecular mobility allows the face-on lamellae to bend in order to reduce the thermodynamic cost of an unfavorable orientation at the top of the film. We predicted the shape of

deformed lamellae by numerical minimization of a simple free-energy model, analogous to descriptions[42–46] of HAN films.

Similarly to HAN, the deformation of lamellae depends on two generic parameters: i) the easy angle $\bar{\theta}_H$ at the free surface and ii) the ratio $H/\bar{L}$, of the film thickness H to the extrapolation length $\bar{L}$. The latter is defined as $\bar{L} = K/W$, where K is an elastic constant proportional to an effective Young modulus E of the lamellar structure. W is the anchoring strength that penalizes deviations of lamella orientation from $\bar{\theta}_H$ at the top of the film. When $\bar{L}$ is substantially larger than H, for example, $H/\bar{L} \sim 0.25$, the deformation of lamellae is weak; in the special case $\bar{\theta}_H = \pi/2$ equilibrium deformations are even impossible (when $H/\bar{L} \leq 1$). In contrast, lamellae bend substantially when $\bar{L}$ is smaller than H.

To cast the generic predictions in terms of actual materials the effect of parameters E, W, $\bar{\theta}_H$, and H must be explicitly considered. For conjugated polymers there are no estimates available for W, but, as a first approximation, one can employ values typical for liquid crystals:[46] $10^{-6} \leq W \leq 10^{-3}$ J m^{-2}. For this range of W, the shape of lamellae crucially depends on elastic constants. For $E \geq 1$ GPa, which is typical for solid, crystalline, lamellae,[55,56] $\bar{L}$ is significantly larger than the practically-relevant

**ADVANCED
SCIENCE NEWS**

www.advancedsciencenews.com

Macro-
Molecular
Rapid Communications

www.mrc-journal.de

range of film thicknesses $H \leqslant 50\,\mathrm{nm}$. Therefore, deformations are negligible. For "softer" Young moduli $E \sim 0.1 - 0.01\,\mathrm{GPa}$, expected in non-solidified mesophases, $\bar{L}$ becomes comparable to, or smaller than, H. In this case, lamellae deform considerably.

We have also considered a scenario where lamellae, instead of simple bending, rearrange into two grains. The first grain presents a group of lamellar layers that are parallel to the free film surface. The second grain occupies the lower part of the film and contains face-on lamellae. We found that a two-layered film is favored thermodynamically only when the anchoring strength associated with the grain boundary is smaller than the anchoring strength at the free surface.

Overall, our qualitative estimates demonstrate the need for further experimental and molecular simulation-based studies of conjugated polymers targeting the elastic properties of their partially-ordered mesophases and thermodynamic parameters of polymer orientation at free surfaces and grain boundaries. In this respect, it might be helpful to consider rod-like oligomers comprising a π-conjugated core with terminal alkyl chains. Liquid-vapor or liquid-solid interfaces mediate their assembly into large 2D crystals[67–69]: sheets with stacks of conjugated cores sandwiched between two layers of terminal chains. In such 2D lamellae, the field of molecular orientations is more easily accessible than in films and, possibly, one could impose competing boundary conditions on opposite edges of the sheet, for example, by proper choice of radiator substrates during assembly by isochoric cooling.[67]

Conflict of Interest

The authors declare no conflict of interest.

Data Availability Statement

The data that support the findings of this study are available from the corresponding author upon reasonable request.

[1] P. Blom, *Adv. Mater. Technol.* **2020**, *5*, 2000144.
[2] A. Salleo, *Mater. Today* **2007**, *10*, 38.
[3] S. R. Forrest, *Nature* **2004**, *428*, 911.
[4] A. Teichler, R. Eckardt, S. Hoeppener, C. Friebe, J. Perelaer, A. Senes, M. Morana, C. J. Brabec, U. S. Schubert, *Adv. Energy Mater.* **2011**, *1*, 105.
[5] N. Stingelin, *Polym. Int.* **2012**, *61*, 866.
[6] C. R. Snyder, R. J. Kline, D. M. DeLongchamp, R. C. Nieuwendaal, L. J. Richter, M. Heeney, I. McCulloch, *J. Polym. Sci., Part B: Polym. Phys.* **2015**, *53*, 1641.
[7] T. J. Prosa, M. J. Winokur, J. Moulton, P. Smith, A. J. Heeger, *Macromolecules* **1992**, *25*, 4364.
[8] M. Brinkmann, *J. Polym. Sci., Part B: Polym. Phys.* **2011**, *49*, 1218.
[9] W. Pisula, M. Zorn, J. Y. Chang, K. Müllen, R. Zentel, *Macromol. Rapid Commun.* **2009**, *30*, 1179.
[10] K. Tremel, S. Ludwigs, in *P3HT Revisited – From Molecular Scale to Solar Cell Devices*, volume 265, (Ed: S. Ludwigs), Springer, Berlin, Heidelberg **2014**, pp. 39–82.
[11] H. Sirringhaus, P. J. Brown, R. H. Friend, M. M. Nielsen, K. Bechgaard, B. M. W. Langeveld-Voss, A. J. H. Spiering, R. A. J. Janssen, E. W. Meijer, P. Herwig, D. M. de Leeuw, *Nature* **1999**, *401*, 685.
[12] H. Yang, S. W. LeFevre, C. Y. Ryu, Z. Bao, *Appl. Phys. Lett.* **2007**, *90*, 172116.
[13] M. Chen, J. R. Niskala, D. A. Unruh, C. K. Chu, O. Lee, J. Fréchet, *Chem. Mater.* **2013**, *25*, 4088.
[14] T. Aubry, A. S. Ferreira, P. Y. Yee, J. C. Aguirre, S. A. Hawks, M. T. Fontana, B. J. Schwartz, S. H. Tolbert, *J. Phys. Chem. C* **2018**, *122*, 15078.
[15] M. R. Hammond, R. J. Kline, A. A. Herzing, L. J. Richter, D. S. Germack, H. W. Ro, C. L. Soles, D. A. Fischer, T. Xu, L. Yu, M. F. Toney, D. M. DeLongchamp, *ACS Nano* **2011**, *5*, 8248.
[16] M. Heeney, I. McCulloch, in *Flexible Electronics: Materials and Applications* (Eds: W. Wong, A. Salleo), Springer Berlin Heidelberg, Berlin, Heidelberg **2009**, pp. 261–296.
[17] I. Osaka, M. Saito, T. Koganezawa, K. Takimiya, *Adv. Mater.* **2014**, *26*, 331.
[18] O. Dolynchuk, P. Schmode, M. Fischer, M. Thelakkat, T. Thurn-Albrecht, *Macromolecules* **2021**, *54*, 5429.
[19] B. Meredig, A. Salleo, R. Gee, *ACS Nano* **2009**, *3*, 2881.
[20] X. Zhang, L. J. Richter, D. M. DeLongchamp, R. J. Kline, M. R. Hammond, I. McCulloch, M. Heeney, R. S. Ashraf, J. N. Smith, T. D. Anthopoulos, B. Schroeder, Y. H. Geerts, D. A. Fische, M. F. Toney, *J. Am. Chem. Soc.* **2011**, *133*, 15073.
[21] V. Skrypnychuk, N. Boulanger, V. Yu, M. Hilke, S. C. B. Mannsfeld, M. F. Toney, D. R. Barbero, *Adv. Funct. Mater.* **2015**, *25*, 664.
[22] N. Boulanger, V. Yu, M. Hilke, M. F. Toney, D. R. Barbero, *Phys. Chem. Chem. Phys.* **2017**, *19*, 8496.
[23] S. Chae, K. H. Cho, S. Won, A. Yi, J. Choi, H. H. Lee, J.-H. Kim, H. J. Kim, *Adv. Mater. Interfaces* **2017**, *4*, 1701099.
[24] J. Rivnay, R. Steyrleuthner, L. H. Jimison, A. Casadei, Z. Chen, M. F. Toney, A. Facchetti, D. Neher, A. Salleo, *Macromolecules* **2011**, *44*, 5246.
[25] M. Li, C. An, T. Marszalek, M. Baumgarten, H. Yan, K. Müllen, W. Pisula, *Adv. Mater.* **2016**, *28*, 9430.
[26] B. O'Connor, R. J. Kline, B. R. Condar, L. Richter, D. Gundlach, M. F. Toney, D. DeLongchamp, *Adv. Funct. Mater.* **2011**, *21*, 3697.
[27] D. Gargi, R. J. Kline, D. M. DeLongchamp, D. A. Fischer, M. F. Toney, B. T. O'Connor, *J. Phys. Chem. C* **2013**, *117*, 17421.
[28] G. Derue, S. Coppée, S. Gabriele, M. Surin, V. Geskin, F. Monteverde, P. Leclére, R. Lazzaroni, P. Damman, *J. Am. Chem. Soc.* **2005**, *127*, 8018.
[29] L. Hartmann, K. Tremel, S. Uttiya, E. Crossland, S. Ludwigs, N. Kayunkid, C. Vergnat, M. Brinkmann, *Adv. Funct. Mater.* **2011**, *21*, 4047.
[30] I. Osaka, K. Takimiya, *Polymer* **2015**, *59*, A1.
[31] V. Skrypnychuk, N. Boulanger, V. Yu, M. Hilke, M. F. Toney, D. R. Barbero, *J. Mater. Chem. C* **2016**, *4*, 4143.

2300437 (10 of 11)

**ADVANCED
SCIENCE NEWS**

www.advancedsciencenews.com

$\{M\}$ acro-
molecular
Rapid Communications

www.mrc-journal.de

[32] D. H. Kim, H. S. Lee, H.-J. Shin, Y.-S. Bae, K.-H. Lee, S.-W. Kim, D. Choi, J.-Y. Choi, *Soft Matter* **2013**, *9*, 5355.

[33] J. Balko, G. Portale, R. H. Lohwasser, M. Thelakkat, T. Thurn-Albrecht, *J. Mater. Res.* **2017**, *32*, 1957.

[34] Y. Y. Yimer, A. Dhinojwala, M. Tsige, *J. Chem. Phys.* **2012**, *137*, 044703.

[35] N. Boulanger, V. Yu, M. Hilke, M. F. Toney, D. R. Barbero, *Phys. Chem. Chem. Phys.* **2018**, *20*, 4422.

[36] M. Ebert, O. Herrmann-Schönherr, J. H. Wendorff, H. Ringsdorf, P. Tschirner, *Liq. Cryst.* **1990**, *7*, 63.

[37] C. Greco, A. Melnyk, K. Kremer, D. Andrienko, K. C. Daoulas, *Macromolecules* **2019**, *52*, 968.

[38] E. L. Wood, C. Greco, D. A. Ivanov, K. Kremer, K. C. Daoulas, *J. Phys. Chem. B* **2022**, *126*, 2285.

[39] D. M. DeLongchamp, R. J. Kline, Y. Jung, E. K. Lin, D. A. Fischer, D. J. Gundlach, S. K. Cotts, A. J. Moad, L. J. Richter, M. F. Toney, M. Heeney, I. McCulloch, *Macromolecules* **2008**, *41*, 5709.

[40] Z. Wu, A. Petzold, T. Henze, T. Thurn-Albrecht, R. H. Lohwasser, M. Sommer, M. Thelakkat, *Macromolecules* **2010**, *43*, 4646.

[41] G. Strobl, *Rev. Mod. Phys.* **2009**, *81*, 1287.

[42] G. Barbero, R. Barberi, *J. Physique* **1983**, *44*, 609.

[43] P. Palffy-Muhoray, E. C. Gartland, J. R. Kelly, *Liquid Crystals* **1994**, *16*, 713.

[44] C. Chiccoli, O. D. Lavrentovich, P. Pasini, C. Zannoni, *Phys. Rev. Lett.* **1997**, *79*, 4401.

[45] C. Chiccoli, P. Pasini, Šarlah A., C. Zannoni, S. Žumer, *Phys. Rev. E* **2003**, *67*, 050703.

[46] M. Kléman, O. D. Lavrentovich, *Soft Matter Physics: An Introduction*, Springer, Berlin, Germany **2002**.

[47] J. Case, A. Chilver, C. Ross, *Strength of Materials and Structures*, Elsevier Ltd., Amsterdam, Netherlands **1999**.

[48] R. P. Feynman, R. B. Leighton, M. Sands, *The Feynman lectures on physics; Definitive ed.*, vol. *2*, Pearson/Addison-Wesley, Boston, USA **2006**.

[49] P. G. de Gennes, J. Prost, *The Physics of Liquid Crystals*, Clarendon Press, Oxford **1995**.

[50] M. Kleman, O. D. Lavrentovich, *Soft Matter Physics: An Introduction*, Springer, Berlin, Germany **2003**.

[51] W. H. Press, S. A. Teukolsky, W. T. Vetterling, B. P. Flannery, *Numerical recipes in C: The Art of Scientific Computing*, 2nd ed., Cambridge University Press, New York **1992**.

[52] P. Ziherl, F. Karimi Pour Haddadan, R. Podgornik, S. Žumer, *Phys. Rev. E* **2000**, *61*, 5361.

[53] S. V. Meille, V. Romita, T. Caronna, A. J. Lovinger, M. Catellani, L. Belobrzeckaja, *Macromolecules* **1997**, *30*, 7898.

[54] D. R. Kozub, K. Vakhshouri, L. M. Orme, C. Wang, A. Hexemer, E. D. Gomez, *Macromolecules* **2011**, *44*, 5722.

[55] B. O'Connor, E. Chan, B. R. Chan, C. Conrad, L. J. Richter, R. J. Kline, M. Heeney, I. McCulloch, C. L. Soles, D. M. DeLongchamp, *ACS Nano* **2010**, *4*, 7538.

[56] K. Jiang, D. Xu, Z. Ma, P. Yang, Y. Song, W. Zhang, *ACS Macro Lett.* **2020**, *9*, 108.

[57] A. Zhugayevych, O. Mazaleva, A. Naumov, S. Tretiak, *J. Phys. Chem. C* **2018**, *122*, 9141.

[58] R. O. Agbaoye, P. O. Adebambo, J. O. Akinlami, T. A. Afolabi, S. Z. Karazhanov, D. Ceresoli, G. Adebayo, *Comput. Mater, Sci.* **2017**, *139*, 234.

[59] E. Jankowski, H. S. Marsh, A. Jayaraman, *Macromolecules* **2013**, *46*, 5775.

[60] H. S. Marsh, E. Jankowski, A. Jayaraman, *Macromolecules* **2014**, *47*, 2736.

[61] V. Y. Rudyak, A. A. Gavrilov, D. V. Guseva, S.-H. Tung, P. V. Komarov, *Mol. Syst. Des. Eng.* **2020**, *5*, 1137.

[62] R. H. Colby, C. K. Ober, J. R. Gillmor, R. W. Connelly, T. Duong, G. Galli, M. Laus, *Rheol. Acta* **1997**, *36*, 498.

[63] A. Selevou, G. Papamokos, M. Steinhart, G. Floudas, *J. Phys. Chem. B* **2017**, *121*, 7382.

[64] S. Shibahara, J. Yamamoto, Y. Takanishi, K. Ishikawa, H. Takezoe, *J. Phys. Soc. Jpn.* **2002**, *71*, 802.

[65] F. Steiner, C. Poelking, D. Niedzialek, D. Andrienko, J. Nelson, *Phys. Chem. Chem. Phys.* **2017**, *19*, 10854.

[66] R. T. Teixeira-Souza, C. Chiccoli, P. Pasini, L. R. Evangelista, C. Zannoni, *Phys. Rev. E* **2015**, *92*, 012501.

[67] V. A. Postnikov, Y. I. Odarchenko, A. V. Iovlev, V. V. Bruevich, A. Y. Pereverzev, L. G. Kudryashova, V. V. Sobornov, L. Vidal, D. Chernyshov, Y. N. Luponosov, O. V. Borshchev, N. M. Surin, S. A. Ponomarenko, D. A. Ivanov, D. Y. Paraschuk, *Cryst. Growth Des.* **2014**, *14*, 1726.

[68] I. Vladimirov, M. Kellermeier, T. Geßner, Z. Molla, S. Grigorian, U. Pietsch, L. S. Schaffroth, M. Kühn, F. May, R. T. Weitz, *Nano Lett.* **2018**, *18*, 9.

[69] V. V. Bruevich, A. V. Glushkova, O. Y. Poimanova, R. S. Fedorenko, Y. N. Luponosov, A. V. Bakirov, M. A. Shcherbina, S. N. Chvalun, A. Y. Sosorev, L. Grodd, S. Grigorian, S. A. Ponomarenko, D. Y. Paraschuk, *ACS Appl. Mater. Interfaces* **2019**, *11*, 6315.